Effect of mechanical boundary conditions on orientation of angiogenic microvessels

Laxminarayanan Krishnan[1], Clayton J. Underwood[1], Steve Maas[1], Benjamin J. Ellis[1], Tejas C. Kode[1], James B. Hoying[2], and Jeffrey A. Weiss[1]*

[1]Department of Bioengineering, University of Utah, 50 South Central Campus Drive, Room 2480, Salt Lake City, UT 84112, USA; and [2]Division of Cardiovascular Therapeutics, Cardiovascular Innovation Institute, University of Louisville, Louisville, KY, USA

Aim Mechanical forces are important regulators of cell and tissue phenotype. We hypothesized that mechanical loading and boundary conditions would influence neovessel activity during angiogenesis.

Methods and resuts Using an *in vitro* model of angiogenesis sprouting and a mechanical loading system, we evaluated the effects of boundary conditions and applied loading. The model consisted of rat microvessel fragments cultured in a 3D collagen gel, previously shown to recapitulate angiogenic sprouting observed *in vivo*. We examined changes in neovascular growth in response to four different mechanical conditions. Neovessel density, diameter, length and orientation were measured from volumetric confocal images of cultures exposed to no external load (free-floating shape control), intrinsic loads (fixed ends, no stretch), static external load (static stretch), or cyclic external load (cyclic stretch). Neovessels sprouted and grew by the third day of culture and continued to do so during the next 3 days of loading. The numbers of neovessels and branch points were significantly increased in the static stretch group when compared with the free-floating shape control group. In all mechanically loaded cultures, neovessel diameter and length distributions were heterogeneous, whereas they were homogeneous in shape control cultures. Neovessels were significantly more oriented along the direction of mechanical loading than those in the shape controls. Interestingly, collagen fibrils were organized parallel and adjacent to growing neovessels.

Conclusion Externally applied boundary conditions regulate neovessel sprouting and elongation during angiogenesis, affecting both neovessel growth characteristics and network morphometry. Furthermore, neovessels align parallel to the direction of stress/strain or internally generated traction, and this may be because of collagen fibril alignment induced by the growing neovessels themselves.

1. Introduction

Physiological organ morphology is achieved by migration and orientation of cells under the influence of chemotaxis, haptotaxis, and mechanotaxis. Both externally applied and internally generated mechanical forces influence cell migratory, proliferative, and secretory activities and matrix orientation.[1–3] The current understanding of the morphogenesis of natural 3D tissue structure is limited. Given its importance in development, repair, tumourigenesis, and design of artificial constructs, significant resources have been directed at understanding the 3D morphology of the microvasculature, especially the vascularity of soft connective tissues,[4,5] where vasculature is often oriented along the direction of strain experienced *in vivo* and/or structural features of the extracellular matrix. Cellular orientation in engineered tissue is often achieved by mechanical loading or contact guidance.[6–9]

Mechanical forces affect the behaviour of nearly all cell types.[7,10–12] The mechanical environment of endothelial cells influences migration, proliferation and tube formation,[11,13] protease and other secretory activities,[14] cellular and cytoskeletal organization,[15] expression of genes and surface molecules,[16] and cell signalling.[12] A large body of literature has focused on the responses of endothelial cells as monolayers, spheroids, or cords, cultured in natural or

* Corresponding Author. Tel: +1 801 587 7834; fax: +1 801 535 6801.
  E-mail address: jeff.weiss@utah.edu

engineered matrices and surfaces, to biochemical and biomechanical stimuli.[11–18] These studies have shown that cells align both along[19,20] and transverse[15,17,18,21] to the direction of principal stretch in response to mechanical loading. The causes of this discrepancy are elusive and have been attributed to cell seeding density, matrix density, genetic framework, cell age, 2D vs. 3D substrates, cell subpopulation and the nature of loading. The angiogenic response of intact preformed microvessels to mechanical perturbations is relatively unexplored.

The objective of the present study was to determine the morphological changes in sprouting microvessels in a 3D *in vitro* model of angiogenesis[22] because of alterations in construct boundary conditions and external loading, in previously unaligned collagen matrices. We quantified the orientation of microvessel segments in free-floating cultures, in cultures under traction against fixed anchors, and in cultures under externally applied strain. This is the first study to examine the orientation of multicellular microvessel structures rather than individual cells or cell clusters. The results of this study demonstrate that neovessel orientation during angiogenesis depends more on culture boundary conditions than on externally applied strains.

2. Methods

2.1 *In vitro* culture model

The 3D *in vitro* angiogenesis model has been characterized in our prior publications.[22,23–25] Unlike angiogenesis models that use isolated endothelial cells, this model uses isolated microvessel fragments. 'Parent' vessels contain associated perivascular cells and retain their basement membrane after initial harvest and seeding in 3D collagen gels. Sprouting begins predictably at Day 2–3. Pericytes disassociate from parent vessels and endothelial cells,

consistent with observations that perivascular cell withdrawal relaxes the parent endothelial cell tube and permits sprouting and vessel elongation during angiogenesis. Sprouts elongate as patent tubes, branching and anastamosing with other vessels, and forming a new vascular network that ultimately fills the construct. Neovessel constructs form a functional vascular tree when implanted,[24] rapidly inosculating with the recipient host circulation after implantation and carrying blood.

Epididymal fat pads from male retired breeder Sprague–Dawley rats (>500 g) were aseptically harvested conforming to the Guide for the Care and Use of Laboratory Animals (NIH Publication No. 85-23, revised 1996) and washed with Leibowitz (L-15) media containing 2% foetal bovine serum. Fat pads were minced into $\sim$1 mm^3 pieces and subjected to limited digestion with 2 mg/mL Clostridium collagenase (Worthington Biochemicals, Lakewood, NJ) and 2 mg/mL bovine serum albumin (BSA, Sigma-Aldrich, St. Louis, MO) in Dulbecco's cation-free phosphate buffered saline (DCF-PBS, pH 7.4) at 37°C for 4 min. The solution was immediately diluted with L-15 media to halt digestion and centrifuged. The pellet was washed twice and resuspended in L-15 media with 2% serum and sequentially filtered through a 350 μm and then a 30 μm sterile nylon filter. The larger filter eliminates undigested particulate debris, whereas the fine filter retains larger vessel fragments, allowing single cells and smaller fragments to pass through. The 30 μm filter was transferred to a sterile Petri dish and washed with serum containing L-15 media to suspend the fragments. The solution was analysed for a number of microvessels and centrifuged to obtain a pellet of microvessel fragments. Reagents were obtained from Invitrogen (Carlsbad, CA) unless mentioned otherwise.

Rat tail collagen type I (BD Biosciences, Bedford, MA) was mixed with concentrated Dulbecco's modified Eagle medium (DMEM, Invitrogen, Carlsbad, CA) to yield a final concentration of 3 mg/mL in $1 \times$ DMEM. Microvessels were suspended in collagen solution at 15000 fragments/mL, and 1.2–1.5 mL of this suspension was pipetted into custom culture chambers and polymerized at 37°C and 95% humidity for 30 min (*Figure 1*). Labtek II chambers (Nunc-Nalge, Rochester, NY) were modified to accommodate a 5 × 20 mm specimen between fixed and mobile anchor posts, based on
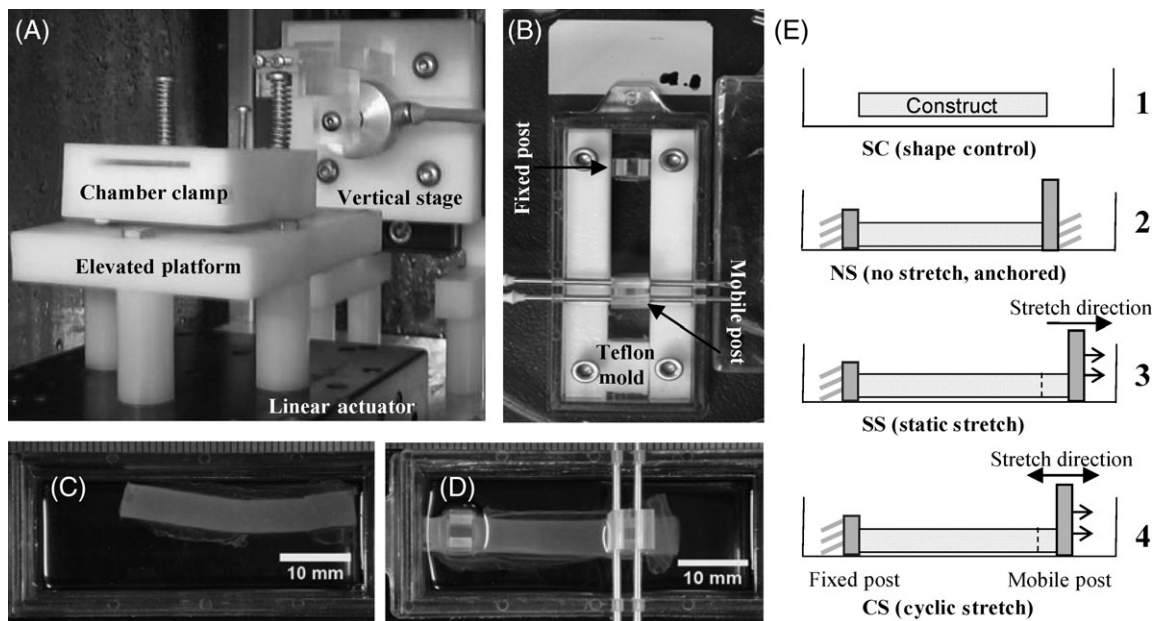
Figure 1 (*A*) Mechanical conditioning system with raised platform mounted on motorized actuator. A stationary vertical stage is interfaced with the mobile anchor post by a beam. (*B*) Modified Labtek culture chamber with fixed anchor, mobile anchor supported by pins and removable Teflon mould. The Teflon mould was removed after collagen polymerization to yield a free-floating tensile test specimen. An unanchored shape control (*C*) and a typical anchored construct (*D*). (*E*) Schematics show the four different test configurations in side view—(1) shape control, (2) no stretch, (3) static stretch and (4) cyclic stretch.
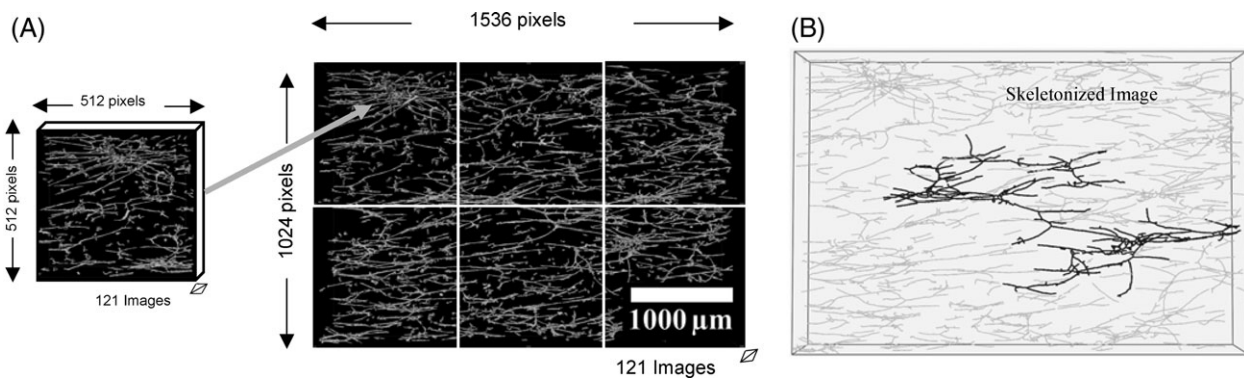
Figure 2 (*A*) Six adjacent confocal image stacks were stitched together to obtain a mosaic of the centre of the construct. (*B*) Final skeletonized output with largest continuous vessel highlighted.

our earlier design.[26] A removable Teflon mould was used to cast the collagen constructs and was then removed after polymerization. The fixed post was attached to the chamber base near one end (Loctite® 3301, Henkel Corp., Rocky Hill, CT). Stainless steel pins were inserted through holes in the sides of the chamber for temporary anchorage of the mobile post. The acrylic posts had holes (1 mm dia) to allow the collagen solution to pass through. Gels were overlaid with serum-free culture media composed of 1:1 mixture of $1 \times$ DMEM (low glucose) and F12 nutrient mixture with additional components (Insulin 5 µg/mL, Transferrin 100 µg/mL, Progesterone 20 nM, Selenium 30 nM, and Putrescine 100 µM),[27] rhVEGF (10 ng/mL, PeproTech, Rocky Hill, NJ), and Gentamycin (50 µg/mL). Three chambers with and one chamber without the acrylic anchors were prepared simultaneously and allowed to grow undisturbed for 3 days. The interval between preparation of microvessel seeded collagen constructs and the beginning of mechanical intervention was based on the time required for initial sprout formation as we previously reported.[22,25] On the third day, culture dimensions were measured with digital calipers, photographed, and given a 70% media change.

2.2 Mechanical conditioning and experimental groups

The mechanical conditioning device used two motorized linear actuators (Aerotech, Pittsburgh, PA, range: ± 25 mm, resolution: ± 5 nm) for simultaneous testing of two constructs within the incubator (*Figure 1A*). Chambers were mounted on raised platforms to minimize any influence of heat, magnetic or electric fields and vibration.

Two conditioning regimens and two boundary conditions were evaluated (*Figure 1E*). For each experiment, one construct was subjected to 6% 'static stretch' (SS group) for 3 days and the second to 6% 'cyclic stretch' (CS group) at 1 Hz for 12 h every 24 h for 3 days. This cyclic routine was chosen since vasculature in tissues that are subjected to cyclic stretch such as muscle and tendon experience a recovery period during the sleep cycle. The free-floating constructs without acrylic anchors, referred to as 'shape control' (SC), were placed on the conditioning platform along with the SS construct. Similarly, the anchored but unstretched construct, referred to herein as 'no stretch' (NS), was placed on the cyclic conditioning platform along with CS construct. To maintain comparability across different groups, four constructs, one for each group, were cast using the same starting material. Some samples became contaminated because of the open culture system and hence the final number of samples in each group over 9 experiments were SC—9, NS—8, SS—6, and CS—6.

2.3 Confocal microscopy

On the sixth day of culture constructs were cut free from the anchor posts with a scalpel, gels were measured and then fixed in 4%

formaldehyde. Note that the fixation caused a reduction in construct volume ($\sim$20% or 7.5% along each dimension, nearly uniform). Microvessels within the gel were permeabilized with 0.1% Triton-X-100 in PBS. Endothelial cells were stained with 2 µg/mL Isolectin IB4-Alexa 488 conjugate (Invitrogen, Carlsbad, CA). Confocal microscopy of six fields adjacent to the centres of the top and bottom surfaces of the constructs was performed on an Olympus FV1000 with a $10 \times$ objective. Individual z-axis images were acquired to a depth of 300 µm at 2.5 µm intervals and 512×512 resolution.

2.4 Volumetric image reconstruction and skeletonization

Image stacks from the six adjacent fields (1.27×1.27 mm each) forming a 2×3 grid were stitched together to generate a single mosaic ($3.8 \times 2.5 \times 300$ mm) (*Figure 2*). The software Amira™ (Mercury Computer Systems, Carlsbad, CA) was used for image analysis and skeletonization. Intensity artefacts in images with slice depth[28] were reduced using an algorithm that fit an exponential curve to average intensities. Mosaic stacks were further deconvolved using a point spread function generated from the numerical aperture (NA = 0.4, 10X—air), wavelength of light (520 nm) and the refractive index of the gel.[29] An automated thresholding algorithm based on a Gaussian distribution fit to the image histogram was used to binarize each mosaic stack (ImageJ, NIH). A size filter of 600 µm³ was applied to remove debris and small cell clusters. Images were then skeletonized.[30,31] A Chamfer distance map was generated as a part of this process, and these data were used to determine average diameter of each segment.[30]

2.5 Data analysis

Coordinates of points from the skeletonization, forming line equivalents of the vasculature, were processed by a custom C++ program (available at http://mrl.sci.utah.edu) to calculate morphometric parameters, including branch points, end points, individual segments, and vessels (all connected segments). Total vascular volume was determined from lengths and diameters. Additional parameters were orientation with respect to stretch axis, segment and total network length, vessel diameters, number of branches, junctions, segments, segment lengths, and vascular volume fractions. A minimum vessel size of 150 µm length was used to avoid smaller segments and debris. This cutoff was based on microvessel dimensions at the time of seeding, which were about 150 µm long. A segment length cutoff of 25 µm was used to eliminate branches that were not much larger than the average vessel diameters. Segment orientation was examined along the direction of stretch (*X*-axis, θ) and through the culture depth (*Z*-axis, δ). Additionally, each segment was projected onto the *XY*-plane and the angle of the projected segment with respect to the *X*-axis was determined (Projected-*X*, ϕ). Segments were sorted into 10° bins from 0–90°.

(A)

(B)
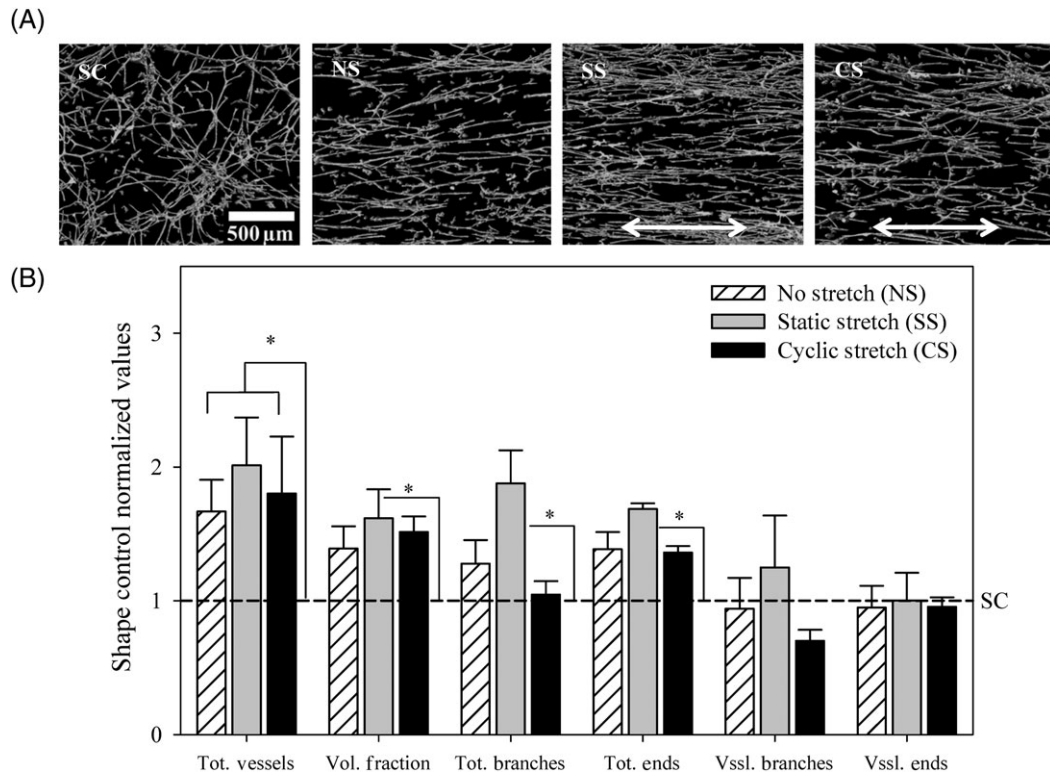
Figure 3 (*A*) 3D images of representative vascularized constructs: SC, shape control; NS, no stretch; SS, static stretch; CS, cyclic stretch. (*B*) Construct vascularity and vascular morphometry measurements, expressed as total number of vessels per construct, volume fraction of total, number of vascular branch points, and end points per construct and per vessel. Values are normalized to values of shape control (abbreviations: Tot, total for entire construct; Vssl, vessel, per continuous vessel; Vol, - volume).

Results were expressed as percentage of total fragments per bin and as percentage of length-weighted segments per bin. The angle distribution of segments was compared between groups and within groups using two-way ANOVAs and Tukey tests (or Kruskal–Wallis ANOVA and Dunn's post hoc tests for nonparametric distributions) with significance at $\alpha = 0.05$.

2.6 Confocal reflectance microscopy

Confocal reflection microscopy[32] was performed to visualize collagen fibril orientation in the presence and absence of anchorage and external loading, and modulation by growing microvessels. Samples were illuminated with a 633 nm laser and reflected light was collected between 632 and 633 nm. Several image stacks (1 µm step size × 50) were collected for each condition. To see whether fibril orientation was induced by the boundary/loading conditions, gels lacking microvessels were prepared and subjected to the same mechanical regimens. After 6 days these gels were fixed while still attached to the anchors.

3. Results

3.1 *In vitro* culture model

All constructs showed well-formed sprouts by Day 3 and well-established vascular networks by Day 6 (*Figure 3A*). Total volume reduction between the third and sixth day of culture was 60% for free-floating SC constructs and 40% for the other three groups ($P = 0.001$, ANOVA). The SC constructs reduced to about 32% of their Day 3 length, whereas the length of constructs in the other groups was maintained by the anchoring posts. The average height reduction in anchored construct groups was 17.6% and not significantly different from the SC constructs. Similarly,

there was 27.6% reduction in the width of the anchored constructs, which was not significantly different from SC constructs. SC constructs showed a near uniform percent contraction along the two directions.

3.2 Construct vascularity and complexity

Microvessel network morphometry at Day 6 was determined from the 3D image reconstructions (*Figure 2*). Qualitatively, the SC constructs showed random microvessel orientation, whereas the NS, SS, and CS constructs showed various degrees of orientation along the construct long axis. The number of vessels per construct was highest in the SS group and lowest in the SC group (*Figure 3B*). All treatment groups had significantly more vessels per construct than the SC group (Kruskal–Wallis ANOVA, $P < 0.05$). Among the three anchored groups, the SS constructs had the highest vessel count, followed by the CS and NS groups. However, these differences were not significant. The vascular volume fraction (construct volume occupied by vessels) of the SS group was 1.62 times higher than the SC group ($P = 0.015$, Tukey post hoc), and the NS and CS groups, were 1.39 and 1.51 times higher, respectively. SS constructs had more branches and vessel ends than the SC group ($P = 0.015$ and $P = 0.003$, respectively, Kruskal–Wallis ANOVA) (*Figure 3B*). There were no differences in branches and endings between any of the anchored (stretched or unstretched) groups. Similarly, average branch points and end points per vessel were not significantly different between treatment groups (one-way ANOVA/Ranks test). The SS group thus showed greater network complexity than SC constructs but was not significantly different in terms of vascular volume
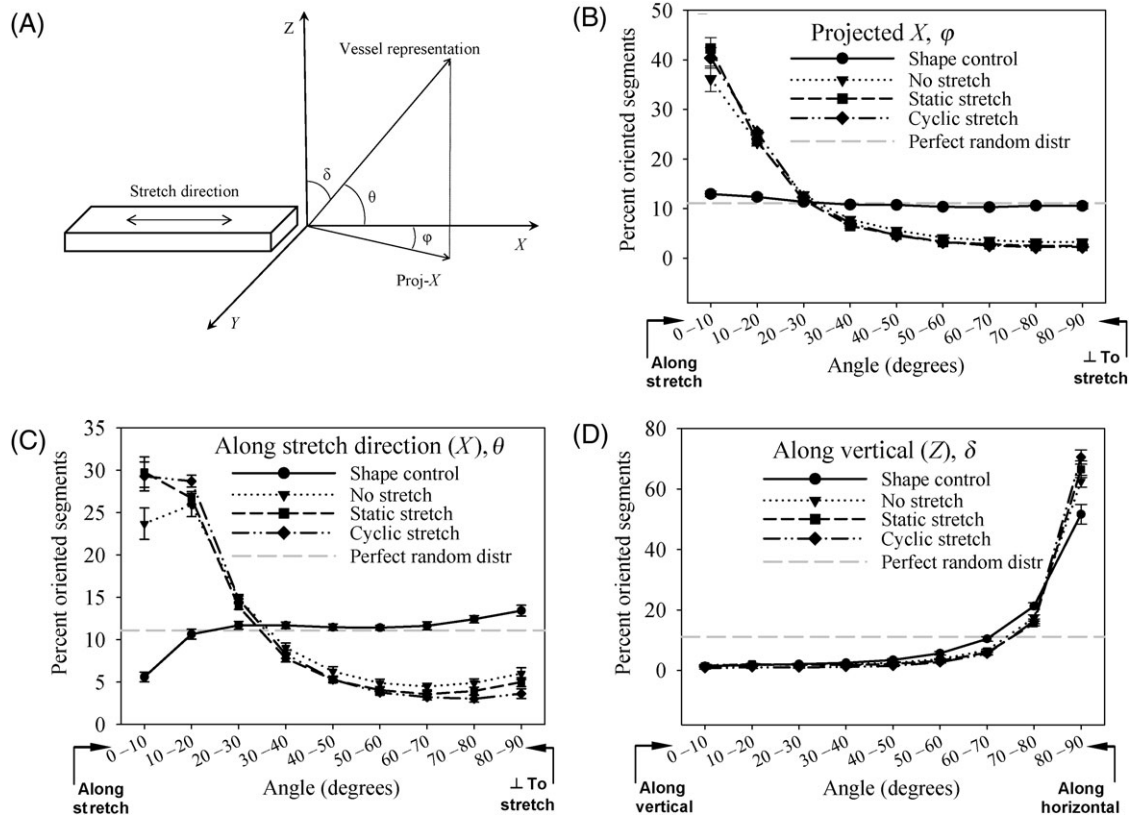
Figure 4 (*A*) Schematic of construct orientation convention. The long axis of the construct was aligned with direction of stretch or anchorage. (*B*) Projection of the segment along the *Z*-axis on the *XY*-plane was used to calculate projected angle (*φ*, Projected-*X*). (*C*) Orientation along *X*-axis (*θ*, horizontal direction of stretch) and (*D*) *Z*-axis (*δ*, vertical transverse to stretch) were directly determined based on segment orientation in these planes.

fraction, branching, and terminations from the other anchored groups.

3.3 Vascular orientation

Preferred orientation of microvessels was observed in the NS, SS, and CS groups (*Figure 4*). In the projected *X*-angle distribution, the SC constructs displayed a random orientation and had a near uniform distribution of segment lengths across all angle bins. Vessel orientation in all anchored constructs was significantly different from the SC (Kruskal–Wallis ANOVA, $P < 0.001$) (*Figure 4B*). In anchored constructs, neovessels aligned with the stretch direction, with approximately 40% of the segments falling in the 0–10° bin. About 70% of segments were oriented along the *X*-axis (0–30°) and the remaining 30% were distributed from 40 to 90°.

Orientation relative to the *X*-axis was similar to the projected *X*-angle distribution, with the SC group being significantly different from the other groups (Kruskal-Wallis ANOVA, $P = 0.003$) and showing nearly equitable distribution of segment lengths across all orientations (*Figure 4C*). Overall a higher percentage of segment lengths of NS, SS, and CS groups was oriented along the stretch direction and lower percentages were oriented orthogonal to stretch than shape controls. Interestingly, irrespective of external boundary conditions, most segments (about 80%) were oriented along the horizontal or *XY*-plane (*Figure 4D*, $P = 0.03$, Kruskal–Wallis ANOVA). In this comparison, the significant difference lies between the SC and CS groups (Dunn's Test, $P < 0.05$), but the general distribution

remained the same for all groups. In all cases, the degree of orientation orthogonal to the vertical direction was significantly greater than that expected for a random distribution (post hoc Tukey, $P < 0.05$) and could explain similarities between results for segment orientation along the *X*-axis and projected *X*-axis. Results without length weighting were similar (data not shown).

3.4 Segment length distribution

There were no significant differences in segment length distribution between groups (Kruskal–Wallis ANOVA, $P = 0.524$) (*Figure 5A*). About 80% of segments were shorter than 100 μm and about 50% were in the 25–50 μm range. Median segment lengths ranged from 53 to 62 μm (*Figure 5A*-Inset). Interestingly, when median segment lengths were analysed as a function of segment orientation, differences were observed between groups (*Figure 5B*, Kruskal–Wallis ANOVA, $P < 0.001$). Anchored groups had longer segments along the direction of stretch or anchorage than the SC group, but were shorter than the shape controls orthogonal to this axis, with a transition point around the 40–50° bin. Vessels in the SS group were significantly shorter than those in the NS and CS groups across all angle bins (multiple comparisons, $P < 0.001$). The SC group did not show significant differences across angle bins, whereas all other groups did show significant differences ($P < 0.001$).

3.5 Segment diameter distribution

There were no significant differences in segment diameter distribution between groups (*Figure 5C*, Kruskal–Wallis
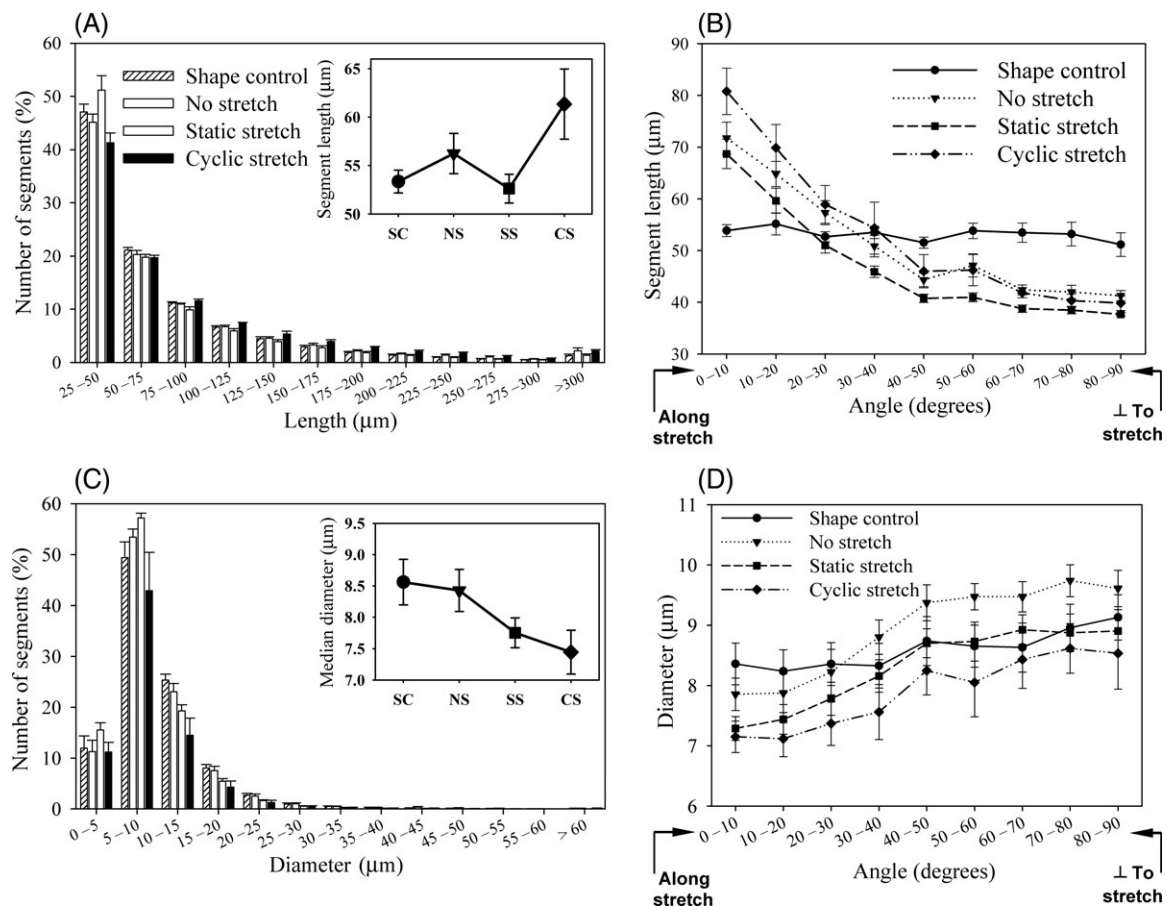
Figure 5 Segment length and diameter distributions. (*A*) Segment length distribution. *Inset*—Median segment lengths over treatment groups. (*B*) Segment length distribution across incremental angle bins. Orientation along the projected *X*-direction is shown. (*C*) Segment diameter distribution within constructs. *Inset*—Median segment diameters over treatment groups. (*D*) Segment diameter distribution across incremental angle bins. Orientation along the projected *X*-direction is shown.

ANOVA, $P = 0.838$). About 70% of segments were less than 10 μm in diameter and nearly 80% were smaller than 15 μm. However, when the distribution of median diameters was examined as a function of segment orientation, there were significant differences between groups (*Figure 5D*, two-way ANOVA, $P < 0.001$). The NS, SS, and CS groups had smaller diameters along the stretch direction, and increasingly larger diameters away from the stretch direction, with the SS (Tukey, $P = 0.002$) and CS (Tukey, $P < 0.001$) groups being significantly thinner than the NS group. Thus, the microvessels were thinner along the direction of stretch and were significantly thinner under the influence of static stretch and cyclic stretch.

## 3.6 Diameter distribution changes with segment length

There was a correlation between median segment diameter and segment length for all groups (data not shown). Longer segments had smaller diameters and vise versa. However, there was a significant effect of mechanical boundary conditions on the distribution of segment diameters with respect to segment lengths (two-way ANOVA, $P < 0.001$). The SS and CS constructs had thinner segments, compared with SC and NS groups (Tukey, $P < 0.001$). Neither the SS and CS nor SC and NS groups differed significantly from each other irrespective of segment lengths.

3.7 Collagen fibre distribution

Since boundary conditions caused neovessel orientation, we examined the structure of the collagen matrix using confocal reflection microscopy (*Figure 6*). Constructs without microvessels were imaged as controls (*Figure 6*, upper panel). In constructs without vessels, fibrils were well defined and randomly oriented in the SC and NS groups. Constructs in the SS and NS groups appeared to have some fibrils with more orientation along the direction of strain. After 6 days *in vitro*, fibrils in constructs containing microvessels were less well defined, likely because of matrix remodelling. Although collagen fibrils were less defined, they appeared to be aligned along the long axis in NS, SS, and CS constructs. Non-anchored SC constructs did not show this orientation.

4. Discussion

The major finding of this work is that boundary conditions and mechanical loading can affect the morphometry of neovessel networks that are formed from angiogenic microvessels in a 3D culture model. Anchoring produced the largest effect in terms of neovessel orientation, whereas static and cyclic mechanical stretch did not cause a significant change in orientation over anchoring alone. To our knowledge this is the first time that the effect of construct
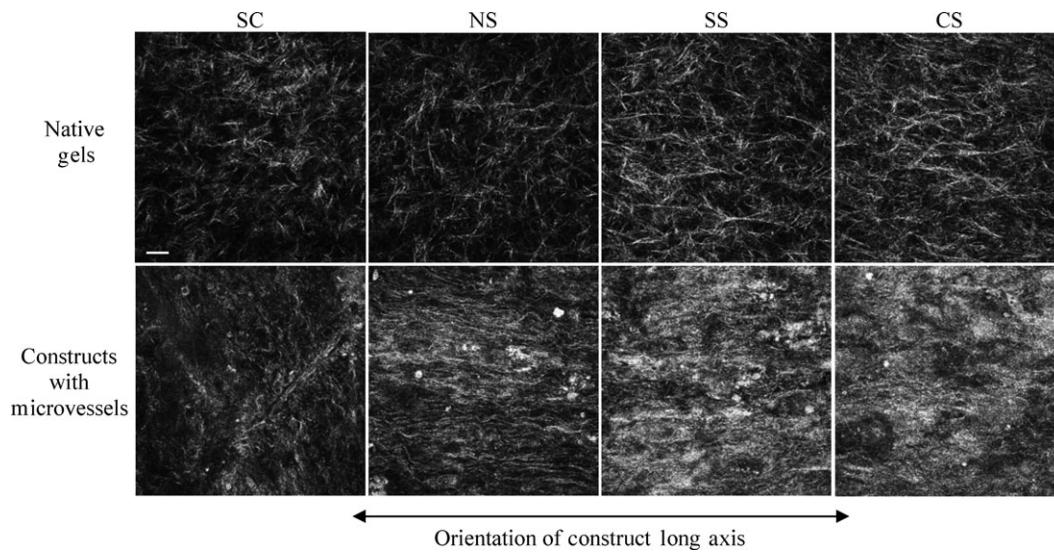
Figure 6 Reorganization of collagen matrix by microvessels. Upper and lower panels contain representative images of the collagen matrix of gels without microvessels and gels with growing microvessels, subjected to identical stretching regimes after 6 days in culture. The collagen matrix in gels containing microvessels is more condensed making the individual collagen fibrils more difficult to distinguish. To eliminate bias because of collagen condensation around microvessels, the images selected for the lower panel do not contain microvessels in those fields. Scale bar in first image = 20 μm. SC, shape control; NS, no stretch; SS, static stretch; CS, cyclic stretch.

anchoring has been demonstrated for angiogenic vessels from preformed microvessels.

Studies of fibroblast cells in 3D culture also observed alignment of collagen fibrils and fibroblasts over time.[6,33] Similarly, long paths of condensed matrix fibres or 'matrix migration pathways' were shown between endothelial cell aggregates or other cell clusters, formed in the direction of overlapping tractional force fields.[1,34–37] Reconstituted collagen gels usually have random orientation. Isolated cells seeded in collagen gels orient along the direction of maximum resistance to deformation by internal traction.[38] These internal contractile forces generated *in vitro* by endothelial cells and fibroblasts are similar to that of dermal fibroblasts and within an order of magnitude of smooth muscle cells.[39,40] The potency of these tractional forces and the formation of capillary-like structures were dependent on monolayer confluence, migratory or quiescent phenotypes, MMP inhibition, substrate properties such as concentration, thickness and rigidity, and anchorage.[35,39,41–43] Cells align with fibrils via contact guidance and generate traction force along the fibre direction, creating a positive feedback loop, ultimately resulting in cell and fibril alignment between anchor points. Such ECM alignment may extend to about 20 μm from cell processes.[2] These observations are supported by several other studies where cellular traction against anchors was sufficient to cause cellular[20] and matrix alignment[1,44] and cell associated fibre bundling.[45] In contrast to those studies that examined alignment of single bipolar cells, the present study examined the orientation of growing microvascular segments, which are multicellular structures.

Cell orientation in an active strain field is generally attributed to an avoidance or shielding response, i.e. the cells tend to orient perpendicular to the direction of stretch.[46,47] Cyclic changes in cell length with axial strain, anisotropic strain fields, anchorage, and relative magnitude of cell traction with respect to the substrate rather than the absolute substrate stiffness have been shown to alter

cellular orientation and modulate capillary morphogenesis.[43,46] In the present study, static and cyclic stretch increased the degree of alignment along the stretch direction; however, the increase over anchoring was minimal and not significant. Thus, these externally applied mechanical strains did not appear to have a significant influence on microvessel orientation. Internal traction forces generated by the microvessels may have been sufficient to induce alignment in the NS group.

The results of this study on multicellular angiogenic microvessels differ from the results of other studies on isolated endothelial cells and fibroblasts.[10,17,18,21,48,49] Endothelial cells grown on 2D elastic substrates orient their primary axis perpendicular to the direction of cyclic strain. In one study, the multicellular cord-like structures formed by invaginations of endothelial cells from surface monolayers into deeper layers of the matrix oriented perpendicular to the direction of cyclic strain,[21] hypothesized to be an attempt to minimize the stress and injury experienced by the cells because of strain at least in 2D settings under cyclic strain. The question thus arises: why do microvessels in collagen gels align along the direction of traction/stretch as opposed to perpendicular to this direction? Possible explanations are that alignment of underlying collagen matrix prevents reorientation by cyclic strain, the viscoelastic nature of collagen gels fail to maintain stress on the cells during the application of the cyclic strain, or that the response of multicellular angiogenic constructs to mechanical strain and fixed tractions is fundamentally different from that of isolated cells on 2D membranes. Although cell reorientation in response to strain has been observed in several studies, the interaction of cells with substrate topology via contact guidance can override this effect.[47] However, matrix alignment does not seem to be the cause of or at least precede cellular alignment under the influence of cyclic stretch.[20] Lower-density collagen gels (1 mg/mL) have been shown to align under the influence of external strain.[50] The results of the present study showed that SC

and NS gels had random fibril orientation, whereas some alignment parallel to stretch direction was observed under static or cyclic strain (*Figure 6*, upper panel). However, alignment is seen in the no stretch group when growing microvessels are present (*Figure 6*, lower panel). Therefore, if anchoring alone can induce the alignment of multicellular neovessels and the collagen matrix, then an addition of cyclic stretch may not be able to reorient cells away from the aligned matrix. The viscoelastic nature of the collagen constructs[26] may also play a role. There may be a fall in the actual tissue equilibrium tension because of stress relaxation, but the gels may still retain a strain-induced collagen alignment.[50] Alignment of endothelial cells, fibroblasts, neurites,[51] and tenocytes[7] on 3D matrices under static or cyclic stretch indicate that cellular tensional homeostasis may play a significant role in 3D tissue architecture development, in conjunction with contact guidance from matrix structure.

We examined vessel volume fraction, segment length, and segment diameter in the microvessel cultures. Although there were no significant differences in volume fraction of vessels across the groups, the average volume fraction across all construct groups (mean = 0.75% of total volume) was similar to those found *in vivo*.[52] Diameter values were in good agreement with previous literature.[53,54] Segment length distributions were broad, but similar to one another with median lengths in a 53–62 μm range. These values are slightly lower than the reported 93 μm in fibrin ingrowth models[54] and 87–119 μm in rat mesenteric capillaries,[55] possibly because of differences in vascular complexity and anastomosis. These observations suggest that this *in vitro* model reasonably replicates the morphometric characteristics of angiogenic microvessels *in vivo*.

It should be noted that diameter measurements from the image data can be influenced by the thresholding process and image resolution. The final voxel resolution of image mosaic stacks (2.5 μm^3) was a function of the $10\times$ objective, the image resolution and Z-direction step size. Although this combination allowed for imaging of a large field of view, the diameter of the vessels was dependent on a small number of voxels. The thresholding process could affect measured diameters; thus an automated thresholding algorithm was used to minimize such errors. Nevertheless, the diameters reported in this study are in good agreement with the literature.[53,54]

Application of engineered grafts in medicine has demonstrated that graft survival is often dependent on the ability to recruit host vasculature. Vascular supply networks to and within an implant form a significant bottleneck in graft integration. A prevascularized graft, engineered to match local vascular topology, tissue architecture, and material properties could provide a solution to this problem. Angiogenesis in a 3D substrate from preformed vascular elements offers a closer approximation to *in vivo* physiological conditions. Our results demonstrate that changing the boundary conditions of a vascularized 3D gel construct can induce substantial organization of angiogenic neovessels. Alignment along the direction of anchorage and strain and the associated perivascular condensed matrix fibrils recapitulate the 3D architecture of soft tissues such as muscles and ligaments.[4,5] Further research is needed to elucidate the changes in gene and protein expression that may be responsible for the observed

phenomena, as well as to quantify changes in collagen fibril morphometry over time.

Acknowledgements

Funding

References

1. Stopak D, Harris AK. Connective tissue morphogenesis by fibroblast traction. I. Tissue culture observations. *Dev Biol* 1982;**90**:383–398.
2. Korff T, Augustin HG. Tensional forces in fibrillar extracellular matrices control directional capillary sprouting. *J Cell Sci* 1999;**112**:3249–3258.
3. Bell E, Ivarsson B, Merrill C. Production of a tissue-like structure by contraction of collagen lattices by human fibroblasts of different proliferative potential in vitro. *Proc Natl Acad Sci USA* 1979;**76**:1274–1278.
4. Bray RC, Fisher AW, Frank CB. Fine vascular anatomy of adult rabbit knee ligaments. *J Anat* 1990;**172**:69–79.
5. Squier CA, Bausch WH. Three-dimensional organization of fibroblasts and collagen fibrils in rat tail tendon. *Cell Tissue Res* 1984;**238**:319–327.
6. Huang D, Chang T, Aggarwal A, Lee R, Ehrlich H. Mechanisms and dynamics of mechanical strengthening in ligament equivalent fibroblast populated collagen matrices. *Ann Biomed Eng* 1993;**21**:289–305.
7. Garvin J, Qi J, Maloney M, Banes AJ. Novel system for engineering bioartificial tendons and application of mechanical load. *Tissue Eng* 2003;**9**:967–979.
8. Dunn GA, Brown AF. Alignment of fibroblasts on grooved surfaces described by a simple geometric transformation. *J Cell Sci* 1986;**83**:313–340.
9. Guido S, Tranquillo RT. A methodology for the systematic and quantitative study of cell contact guidance in oriented collagen gels. Correlation of fibroblast orientation and gel birefringence. *J Cell Sci* 1993;**105**:317–331.
10. Neidlinger-Wilke C, Grood E, Claes L, Brand R. Fibroblast orientation to stretch begins within three hours. *J Orthop Res* 2002;**20**:953–956.
11. Von Offenberg Sweeney N, Cummins PM, Cotter EJ, Fitzpatrick PA, Birney YA, Redmond EM et al. Cyclic strain-mediated regulation of vascular endothelial cell migration and tube formation. *Biochem Biophys Res Commun* 2005;**329**:573–582.
12. Azuma N, Duzgun SA, Ikeda M, Kito H, Akasaka N, Sasajima T et al. Endothelial cell response to different mechanical forces. *J Vasc Surg* 2000;**32**:789–794.
13. Li W, Sumpio BE. Strain-induced vascular endothelial cell proliferation requires PI3K-dependent mTOR-4E-BP1 signal pathway. *Am J Physiol Heart Circ Physiol* 2005;**288**:H1591–H1597.
14. Sumpio BE, Banes AJ, Link GW, Iba T. Modulation of endothelial cell phenotype by cyclic stretch: inhibition of collagen production. *J Surg Res* 1990;**48**:415–420.
15. Iba T, Sumpio BE. Morphological response of human endothelial cells subjected to cyclic strain in vitro. *Microvasc Res* 1991;**42**:245–254.
16. Chen BP, Li YS, Zhao Y, Chen KD, Li S, Lao J et al. DNA microarray analysis of gene expression in endothelial cells in response to 24-h shear stress. *Physiol Genomics* 2001;**7**:55–63.
17. Moretti M, Prina-Mello A, Reid AJ, Barron V, Prendergast PJ. Endothelial cell alignment on cyclically-stretched silicone surfaces. *J Mater Sci Mater Med* 2004;**15**:1159–1164.
18. Shirinsky VP, Antonov AS, Birukov KG, Sobolevsky AV, Romanov YA, Kabaeva NV et al. Mechano-chemical control of human endothelium orientation and size. *J Cell Biol* 1989;**109**:331–339.
19. Haston WS, Shields JM, Wilkinson PC. The orientation of fibroblasts and neutrophils on elastic substrata. *Exp Cell Res* 1983;**146**:117–126.
20. Eastwood M, Mudera VC, McGrouther DA, Brown RA. Effect of precise mechanical loading on fibroblast populated collagen lattices: morphological changes. *Cell Motil Cytoskeleton* 1998;**40**:13–21.

21. Joung IS, Iwamoto MN, Shiu YT, Quam CT. Cyclic strain modulates tubulo-genesis of endothelial cells in a 3D tissue culture model. *Microvasc Res* 2006;**71**:1–11.

22. Hoying JB, Boswell CA, Williams SK. Angiogenic potential of microvessel fragments established in three-dimensional collagen gels. *In Vitro Cell Dev Biol Anim* 1996;**32**:409–419.

23. Kirkpatrick ND, Andreou S, Hoying JB, Utzinger U. Live imaging of collagen remodeling during angiogenesis. *Am J Physiol Heart Circ Physiol* 2007;**292**:H3198–H3206.

24. Shepherd BR, Chen HY, Smith CM, Gruionu G, Williams SK, Hoying JB. Rapid perfusion and network remodeling in a microvascular construct after implantation. *Arterioscler Thromb Vasc Biol* 2004;**24**:898–904.

25. Krishnan L, Hoying JB, Nguyen H, Song H, Weiss JA. Interaction of angiogenic microvessels with the extracellular matrix. *Am J Physiol Heart Circ Physiol* 2007;**293**:H3650–H3658.

26. Krishnan L, Weiss JA, Wessman MD, Hoying JB. Design and application of a test system for viscoelastic characterization of collagen gels. *Tissue Eng* 2004;**10**:241–252.

27. Bottenstein JE, Sato GH. Growth of a rat neuroblastoma cell line in serum-free supplemented medium. *Proc Natl Acad Sci USA* 1979;**76**:514–517.

28. Dey N, Blanc-Feraud L, Zimmer C, Roux P, Kam Z, Olivo-Marin JC *et al.* Richardson-Lucy algorithm with total variation regularization for 3D confocal microscope deconvolution. *Microsc Res Tech* 2006;**69**:260–266.

29. Liu Y, Griffith M, Watsky MA, Forrester JV, Kuffova L, Grant D *et al.* Properties of porcine and recombinant human collagen matrices for optically clear tissue engineering applications. *Biomacromolecules* 2006;**7**:1819–1828.

30. Fouard C, Malandain G, Prohaska S, Westerhoff M. Blockwise processing applied to brain microvascular network study. *IEEE Trans Med Imaging* 2006;**25**:1319–1328.

31. Cassot F, Lauwers F, Fouard C, Prohaska S, Lauwers-Cances V. A novel three-dimensional computer-assisted method for a quantitative study of microvascular networks of the human cerebral cortex. *Microcirculation* 2006;**13**:1–18.

32. Brightman AO, Rajwa BP, Sturgis JE, McCallister ME, Robinson JP, Voytik-Harbin SL. Time-lapse confocal reflection microscopy of collagen fibrillogenesis and extracellular matrix assembly in vitro. *Biopolymers* 2000;**54**:222–234.

33. Girton TS, Barocas VH, Tranquillo RT. Confined compression of a tissue-equivalent: collagen fibril and cell alignment in response to anisotropic strain. *J Biomech Eng* 2002;**124**:568–575.

34. Vernon RB, Sage EH. Between molecules and morphology. Extracellular matrix and creation of vascular form. *Am J Pathol* 1995;**147**:873–883.

35. Vernon RB, Angello JC, Iruela-Arispe ML, Lane TF, Sage EH. Reorganization of basement membrane matrices by cellular traction promotes the formation of cellular networks in vitro. *Lab Invest* 1992;**66**:536–547.

36. Lo CM, Wang HB, Dembo M, Wang YL. Cell movement is guided by the rigidity of the substrate. *Biophys J* 2000;**79**:144–152.

37. Davis GE, Camarillo CW. Regulation of endothelial cell morphogenesis by integrins, mechanical forces, and matrix guidance pathways. *Exp Cell Res* 1995;**216**:113–123.

38. Bischofs IB, Schwarz US. Cell organization in soft media due to active mechanosensing. *Proc Natl Acad Sci USA* 2003;**100**:9274–9279.

39. Vernon RB, Sage EH. Contraction of fibrillar type I collagen by endothelial cells: a study in vitro. *J Cell Biochem* 1996;**60**:185–197.

40. Kolodney MS, Wysolmerski RB. Isometric contraction by fibroblasts and endothelial cells in tissue culture: a quantitative study. *J Cell Biol* 1992;**117**:73–82.

41. Ingber DE, Folkman J. Mechanochemical switching between growth and differentiation during fibroblast growth factor-stimulated angiogenesis in vitro: role of extracellular matrix. *J Cell Biol* 1989;**109**:317–330.

42. Deroanne CF, Lapiere CM, Nusgens BV. In vitro tubulogenesis of endothelial cells by relaxation of the coupling extracellular matrix-cytoskeleton. *Cardiovasc Res* 2001;**49**:647–658.

43. Sieminski AL, Hebbel RP, Gooch KJ. The relative magnitudes of endothelial force generation and matrix stiffness modulate capillary morphogenesis in vitro. *Exp Cell Res* 2004;**297**:574–584.

44. Delvoye P, Wiliquet P, Leveque JL, Nusgens BV, Lapiere CM. Measurement of mechanical forces generated by skin fibroblasts embedded in a three-dimensional collagen gel. *J Invest Dermatol* 1991;**97**:898–902.

45. Porter RA, Brown RA, Eastwood M, Occleston NL, Khaw PT. Ultrastructural changes during contraction of collagen lattices by ocular fibroblasts. *Wound Repair Regen* 1998;**6**:157–166.

46. Neidlinger-Wilke C, Grood ES, Wang J-C, Brand RA, Claes L. Cell alignment is induced by cyclic changes in cell length: studies of cells grown in cyclically stretched substrates. *J Orthop Res* 2001;**19**:286–293.

47. Wang JH, Grood ES. The strain magnitude and contact guidance determine orientation response of fibroblasts to cyclic substrate strains. *Connect Tissue Res* 2000;**41**:29–36.

48. Ives CL, Eskin SG, McIntire LV. Mechanical effects on endothelial cell morphology: in vitro assessment. *In Vitro Cell Dev Biol* 1986;**22**:500–507.

49. Wang JH, Goldschmidt-Clermont P, Wille J, Yin FC. Specificity of endothelial cell reorientation in response to cyclic mechanical stretching. *J Biomech* 2001;**34**:1563–1572.

50. Voytik-Harbin SL, Roeder BA, Sturgis JE, Kokini K, Robinson JP. Simultaneous mechanical loading and confocal reflection microscopy for three-dimensional microbiomechanical analysis of biomaterials and tissue constructs. *Microsc Microanal* 2003;**9**:74–85.

51. Bray D. Axonal growth in response to experimentally applied mechanical tension. *Dev Biol* 1984;**102**:379–389.

52. Anwar M, Weiss J, Weiss HR. Quantitative determination of morphometric indices of the total and perfused capillary network of the newborn pig brain. *Pediatr Res* 1992;**32**:542–546.

53. Rieder MJ, O'Drobinak DM, Greene AS. A computerized method for determination of microvascular density. *Microvasc Res* 1995;**49**:180–189.

54. Brey EM, King TW, Johnston C, McIntire LV, Reece GP, Patrick CW Jr. A technique for quantitative three-dimensional analysis of microvascular structure. *Microvasc Res* 2002;**63**:279–294.

55. Norrby K. Microvascular density in terms of number and length of microvessel segments per unit tissue volume in mammalian angiogenesis. *Microvasc Res* 1998;**55**:43–53.